Journal of Power Sources 469 (2020) 228378

Contents lists available at ScienceDirect

Journal of Power Sources

journal homepage: www.elsevier.com/locate/jpowsour

Gel electrolyte for a 4V flexible aqueous lithium-ion battery

Arthur Cresce [a,*], Nico Eidson [a,b], Marshall Schroeder [a], Lin Ma [a], Yakira Howarth [a], Chongyin Yang [b], Janet Ho [a], Robert Dillon [a], Michael Ding [a], Alexander Bassett [c], Joseph Stanzione [c], Robinson Tom [d], Thiagarajan Soundappan [d], Chunsheng Wang [b], Kang Xu [a]

[a] US Army Research Laboratory, 2800 Powder Mill Road, Adelphi, MD, 20783, USA
[b] University of Maryland, College Park, MD, 20740, USA
[c] Rowan University, 201 Mullica Hill Rd, Glassboro, NJ, 08028, USA
[d] Navajo Technical University, Lowerpoint Road State Hwy 371, Crownpoint, NM, 87313, USA

HIGHLIGHTS

- UV-cured gel electrolytes were used to construct a 4 V lithium ion battery.
- The main gel electrolyte was water-based, making the battery safe.
- Gel electrolytes had conductivity ≥0.3 mS/cm.
- Gel electrolytes exhibited favorable impedance characteristics.
- Battery cells used graphite anodes and $LiCoO_2$ cathodes.

ARTICLE INFO

Keywords:
Lithium-ion
High voltage
Aqueous electrolyte
Gel electrolyte
Ultraviolet cure
Safety

ABSTRACT

A system of electrolytes using water as a solvent was successfully used to support a typical lithium-ion battery chemistry that operates at 3.7V–4.2 V using standard ultraviolet-cured acrylic-based polymers as hydrophobic barriers. The aqueous electrolyte is contained in a system of poly(ethylene glycol) acrylate polymers crosslinked to produce an electrolyte gel that has electrochemical properties similar to that of the liquid phase component. The electrolyte gels have elastic moduli in the kPa range, making them soft enough to tolerant flexing, cutting, and blunt force impacts while keeping the electrodes covered and safe from shorting. While batteries based on water-in-salt electrolyte provides intrinsic safety that is otherwise unavailable from typical non-aqueous electrolytes, acrylate-based aqueous gel electrolytes offer the potential of large-scale manufacturing owing to the relatively low volatility of the electrolyte components and the low complexity of the proposed manufacturing process.

1. Introduction

The work described in this article details efforts to produce a 4 V class aqueous-based lithium-ion battery using a manufacturing-friendly acrylate gel electrolyte system. The aqueous 4 V battery system combines the inherent safety of high concentration aqueous electrolytes along with the developing concept of hydrophobic anode protection to enable the use of state-of-the-art anode materials that operate at or near the Li/Li^+ potential.

Gel electrolytes are a common feature of diverse and important electrochemical systems. Mass-produced Ag/AgCl reference electrodes frequently have the AgCl-coated Ag wire embedded in a cellulose or poly (vinyl alcohol) gel with a saturated solution of KCl [1–4]. The same strategy of gel electrolytes is used in pH sensing electrodes. For reference electrodes, the gel slows the leakage of the reference electrolyte into the test solution, resulting in a cheap, easy-to-manufacture device and a more sample-stable reference potential. Dye-sensitized solar cells (Grätzel cells) often employ a polymer matrix to form a gel polymer electrolyte used to transfer an electron in a redox couple from the counter electrode to the ionized dye in the anode side [5,6]. Electrochemical Clark cell sensors use a layer of a cellulose acetate or gelatin to immobilize an electrolyte solution used to detect potential changes

* Corresponding author.
E-mail address: arthur.v.cresce.civ@mail.mil (A. Cresce).

https://doi.org/10.1016/j.jpowsour.2020.228378
Received 15 April 2020; Received in revised form 5 May 2020; Accepted 18 May 2020
Available online 8 June 2020
0378-7753/Published by Elsevier B.V.

related to the content of oxygen dissolved in the electrolyte that can react with a platinum cathode [7]. Each of these instances take advantage of the fact that the gel electrolyte restricts the liquid phase to a defined volume, enabling simple fabrication and limiting the contact of electrolyte with other system components.

The use of gel electrolytes in lithium-ion batteries reaches back to the work of Michel Armand in the late 1970s – early 1980s with his publications relating to the use of salts dissolved in solid polymers [8,9] and has expanded to today's wide market for gel electrolytes in lithium polymer batteries (LiPo, LIP, etc.). These electrolytes typically use a polymer matrix of poly(vinylidene fluoride), poly(ethylene oxide), and poly(acrylonitrile), among others. These gel electrolytes have sufficient Li^+ conductivities of ≥0.1 mS/cm [10–12] and are used in a wide variety of applications such as high-power remote-controlled vehicles, personal electronics, and in some electric vehicles. The advantage lithium polymer batteries have is the containment of the liquid electrolyte by the gel and reduced need for rigid or bulky packaging. Despite advantages in packaging and energy density, lithium polymer batteries use a standard liquid carbonate-based electrolyte with $LiPF_6$ as a salt, and are therefore still subject to gassing, cell expansion, and fires which result from cell aging processes and direct penetrating or non-penetrating damage to the cell.

A lithium-ion battery with a 4 V operating potential and a non-flammable water-LiTFSI electrolyte has several advantages over batteries with carbonate electrolytes using $LiPF_6$ salt. LiTFSI decomposes close to but before its typically stated melting point of 236 °C, enabling water/LiTFSI aqueous cells to be operated above 70 °C with no salt thermal decomposition and at high temperatures inaccessible to $LiPF_6$-containing electrolytes. An aqueous cell could expect to reduce pack mass by at least 15% with reductions in the thickness of individual cell containment, cooling systems, and fire protection materials, boosting energy density of typical electrode combinations up to 300 Wh/kg. Recently our collaborative group reported a graphite cathode intercalated with bromide/chloride ions that delivered 243 mAh/g at 4.1 V, leading to projections of pack energy density of 400 Wh/kg [13]. Combining high energy density with intrinsic materials-level safety gave our group reason to improve the manufacturing of aqueous lithium-ion batteries using gel electrolytes.

In 2015, our collaborative group first introduced the concept of a "water-in-salt" (WiSE) electrolyte [14], showing that a solution of 21 mol/kg (molal) of lithium bis(trifluoromethanesulfonyl)imide (LiTFSI) in water could increase the electrochemical stability window of a water solution to 3 V, double the practical limit of 1.5 V frequently found in batteries using an aqueous chemistry (alkaline, lead-acid, NiCd, NiMH). The high stability of the LiTFSI:water system is a combination of solid electrolyte interphase (SEI) formation through $TFSI^-$ anion reduction and a relative lack of "free" or non-coordinating water molecules in solution. It was found that aqueous electrolyte electrochemical stability could be increased by adding a co-solvent to water, resulting in what was termed a hybrid aqueous/non-aqueous electrolyte (HANE) [15]. HANE also reduced the amount of costly LiTFSI salt used in the electrolyte. A shortcoming of WiSE and its HANE derivatives is that the electrochemical stability window is not symmetrical across the standard hydrogen electrode (SHE) potential; rather it is more stable against oxidation, shifting stability towards cathodes and away from anodes in a situation termed the "cathodic challenge." Fig. 1 depicts this stability imbalance. In the cathodic challenge, water-solvated Li^+ is delivered to the negative electrode when charging potential is applied to the cell [16].

The coordination between water and Li^+ is strong [16,17], therefore Li^+ brings its coordinating water molecules close enough to the anode surface to be reduced to H_2. Effectively, this meant that high salt concentration and co-solvent addition could not stabilize WiSE against an anode like graphite, silicon, or lithium metal, limiting cell energy density to 90 Wh/kg based on a $Li_4Ti_5O_{12}$:$LiMn_2O_4$ electrode pair and 165 Wh/kg based on a $Li_4Ti_5O_{12}$:$LiNi_{0.5}Mn_{1.5}O_4$ electrode pair. The lack of accessible high energy anodes posed a significant hurdle for WiSE to be used in batteries for mobile electronic devices and transportation applications.

The solution to this problem was to apply a hydrophobic electrolyte to the anode surface which would mediate the interface between the WiSE electrolyte and a graphite anode [18]. This hydrophobic electrolyte was designed to act as an extended solid electrolyte interphase (SEI) layer, passivating the graphite and retarding the movement of water to the graphite during charging. The effect of the hydrophobic electrolyte on overall electrolyte stability can be seen in Fig. 1, where the effective electrolyte stability extends fully to the Li/Li^+ potential. Anode protection allowed a graphite:$LiMn_2O_4$ 4 V battery to go through more than 200 charge/discharge cycles before 80% original capacity was reached [18].

In order to make 4 V batteries using aqueous electrolytes feasible for manufacture, we considered the use of acrylate-based gel electrolytes.

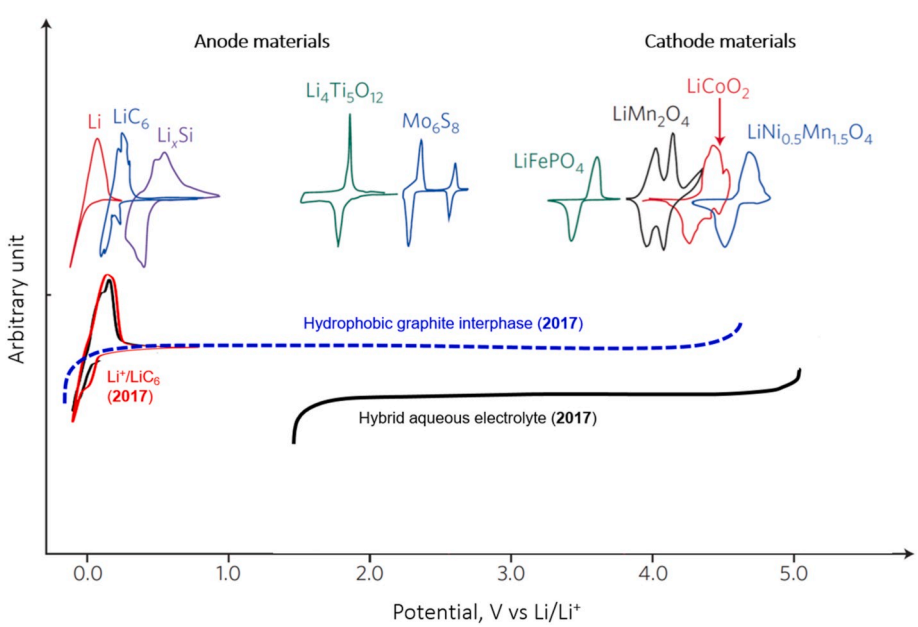

Fig. 1. Schematic depiction of the cathodic challenge faced by aqueous electrolytes along with CV representations of various anodes and cathodes. The hybrid aqueous electrolyte (black) maintains stability against water oxidation but has insufficient cathodic stability to perform Li^+ charge transfer at anodes such as graphite, silicon, and lithium metal. The 2017 innovation of hydrophobic anode protection (blue, dotted) bridged the gap between LTO ($Li_5Ti_4O_{12}$) and silicon anodes, allowing the assembly of a non-flammable 4 V aqueous-based lithium-ion battery cell. (For interpretation of the references to color in this figure legend, the reader is referred to the Web version of this article.)

Acrylic polymers are durable and are available with a large variety of side group functionalities for different applications. They are a mainstay of modern cured-ink printing techniques [19,20]. Acrylates and methacrylates can be initiated to polymerize and crosslink through ultraviolet irradiation (among many other methods not discussed here), and polymerization propagates through a radical chain-growth mechanism. Radical polymerization can occur in a variety of solutions due to the high reactivity of the initiated radical and the relatively high rate of propagation compared to rates of chain transfer and termination. The expression typically used to describe the polymerization rate R_p of a radical polymerization is given as:

$$R_p = k_p (f k_d / k_t)^{1/2} \, [I]^{1/2} [M] e^{-k_d t/2} \tag{1}$$

During this work, it was found that WiSE and its derivatives have low UV absorption in the range of 225 nm–400 nm, and have high propagation rates and fast polymerization times of less than 10 s. WiSE and its derivatives appear to be poor radical scavengers that do not significantly reduce the initiator dissociation constant k_d or increase the termination rate constant k_t through reaction medium-effected recombination/disproportionation. Because of this, k_p is sufficiently large compared to k_t and radical polymerization proceeds in WiSE and its derivatives, resulting in solid electrolyte gels. These gels accomplish several key tasks in the 4 V aqueous lithium-ion battery cell: (1) they physically contain the liquid part of the gel electrolyte, (2) they provide separator function and prevent electrode shorting due to abuse, and (3) they allow facile processing of cell components with a library of side group functionalities (PEGs, fluorinated alkyls, silanes, etc.) for customization and optimization of mechanical and electrochemical properties. In this work, we will detail the development of a 4 V aqueous lithium-ion battery that uses acrylate gel electrolytes to demonstrate the concept of gel electrolytes in a functional cell. Tweaks to electrode design made in concert with electrolyte gel improvements are expected to produce aqueous-based lithium-ion batteries that can deliver energy densities in excess of 300 Wh/kg.

2. Materials and methods

2.1. Electrolyte preparation

The hybrid electrolyte of water:trimethylphosphate, called HT-29 (a 2:9 mass ratio of H_2O to TMP), was prepared by mixing 146.34 g of LiTFSI (Solvay) with 9.76 g water that was purified to 18.2 MΩ by a Millipore A10 water purification system and 43.903 g of trimethylphosphate (TMP) (Millipore-Sigma). The resulting mixture was sealed, sonicated for 1 h, and stored at 50 °C, resulting in a clear, colorless, viscous electrolyte solution. The mole ratio of the components LiTFSI: water:TMP is therefore approximately 37:40:23. Non-aqueous ("anode protection") electrolytes were prepared in a Vacuum Atmospheres Nexus 1 glovebox filled with argon gas and controlled to less than 1 ppm of water and 1 ppm of oxygen. Fluoroethylene carbonate (FEC) (Gotion) was dried over molecular sieves and stored in the glovebox. Trifluoroethyl methyl carbonate (FEMC) (Synquest) was dried over molecular sieves and stored in the glovebox. Karl-Fisher titration determined that the water level of both non-aqueous solvents was less than 24 ppm. A liquid electrolyte with the composition FEC:FEMC 1:1 by mass with 1 m LiTFSI was prepared in the glovebox, sealed, and moved to the dryroom for cell construction.

2.2. Cell construction

2.2.1. Dry materials

Graphite and $LiCoO_2$ (LCO) electrodes were prepared by Saft America, stored in an argon glovebox, and baked at 80 °C under vacuum before cell assembly in a dryroom with a dewpoint of −40 °C. Graphite anodes were 95 wt% proprietary Saft graphite and 5 wt% PTFE binder, and LCO cathodes were 90 wt% LCO, 5 wt% PVdF binder, and 5 wt% carbon black. Electrodes were punched into a rectangular shape 3.8 cm × 6.6 cm with a left-side tab using an MTI hydraulic precision die cutter, giving a total electrode area of 25.08 cm^2. A 4 cm nickel tab was welded onto the short exposed electrode tab using a Sonobond Dual Head Ultrasonic Metal Spot Welder operated at the 25 W setting. Aluminum laminated pouch material (MTI) was cut into 8 cm × 6 cm sheets and used to contain the cured electrode-electrolyte pairs. Areal capacity of the cathode was 1.2 mAh/cm^2 with anode capacity matched at 1.1 mAh/cm [2]. Maximum theoretical capacity of the cell was therefore 27.59 mAh.

2.2.2. Wet materials

Cathode gel electrolyte was prepared by mixing a solution of poly (ethylene glycol) methyl ether acrylate (MPEGA) (Millipore-Sigma, average M_w ~ 480), hydroxyethyl acrylate (HEA) (Millipore-Sigma), and the crosslinker poly(ethylene glycol) diacrylate (PEGDA700) (Millipore-Sigma, average M_w ~ 700) with a mass ratio of MPEGA:HEA: PEGDA700 89:9:2. The photoinitiator 2,2-dimethoxy-2-phenylacetophenone (DMPA) (Millipore-Sigma) was used at a concentration of 0.2 mass % in the monomer/crosslinker solution, resulting in a pre-gel solution ready to undergo ultraviolet (UV) initiation and gel formation. The complete cathode pre-gel solution was mixed with the HT-29 electrolyte with a mass ratio of 25:75 pre-gel:HT-29. The cathode pre-gel solution cures to a soft, springy, and sticky gel.

Anode electrolyte gels were prepared by mixing the same monomer and crosslinker components in the ratio of MPEGA:HEA:PEGDA700 86:7:7, with 0.2 mass % DMPA initiator added to the monomer/crosslinker solution. The complete anode pre-gel solution was mixed with FEC:FEMC 1:1 1 m LiTFSI with a mass ratio of 25:75 pre-gel:electrolyte.

Electrodes were laid flat on sheets of fluorinated silicone rubber (McMaster) cleaned by isopropanol, making them tacky and able to temporarily flatten the one-side-coated electrodes for film casting. Alongside the electrodes was laid two parallel strips of kapton tape with a film thickness of 160 μm with a spacing of 5 cm to allow space for the electrode and some overfill for edge short protection. Electrode and current collectors were measured to have a sum thickness of ~90 μm, giving a total gel thickness of 70 μm. This setup was used for both anodes and cathodes, giving a total gel electrolyte thickness of 140 μm and a total stack thickness of 320 μm.

Cathodes were cured by applying ~1 mL of anode pre-gel solution onto the LCO anode. The wetted LCO electrode was then loaded into a small vacuum chamber and evacuated for 2 min to encourage maximum wetting of the anode by the electrolyte, during which significant bubbles escaped from the cathode and into the pre-gel solution. After 2 min, ambient pressure is gently restored and a PTFE tape-coated glass slide is placed on the Kapton tape over the wet electrode, taking care not to trap air bubbles under the glass. The PTFE coating was used to prevent the gel electrolyte from sticking to the glass slide, easing removal after curing was completed. The covered and vacuum-filled electrode was then immediately placed in a Uvitron Rayven sample chamber set at a 6 cm lamp-to-sample distance resulting in an approximate delivered power of 180 mW/cm^2 to the sample surface. UV was generated by a Uvitron SkyRay 600 W mercury vapor lamp. Exposure time was 60 s. The cured electrode with gel electrolyte was then carefully separated from the PTFE-glass cover and set aside placed on a previously cut laminated aluminum sheet to await joining with the cured anode.

Anodes were cured by applying ~1 mL of anode pre-gel solution onto the graphite anode and placing a rectangle of Celgard 2400 4 cm × 0.5 cm across the top of the anode surface, which saturates the Celgard. The purpose of the Celgard was to prevent shorts caused by rough areas around the tab weld. The wetted electrode was then loaded into a small vacuum chamber and evacuated for 2 min to encourage maximum wetting of the anode by the electrolyte. After 2 min, ambient pressure was gently restored and a PTFE tape-coated glass slide is placed on the Kapton tape over the wet electrode, taking care not to trap air bubbles

under the glass. The covered and vacuum-filled electrode was then cured for 60 s at the same 6 cm separation as the cathode to apply 180 mW/cm^2. The cured electrode with gel electrolyte was then carefully separated from the PTFE-glass cover and placed on a previously cut laminated aluminum sheet with enough space on all sides so that heat-sealing of the pouch would not heat the cell stack. The cured cathode was then placed over the anode, taking care to precisely place the cathode on the center of the anode and to align the tabs in parallel. Hot melt adhesive was then placed across the tabs where they protrude from the pouch, and a Miller 12-inch manual double hand sealer was used to seal across the tabs and down the long sides of the pouch. A double-sided vacuum sealer was used to complete the construction of the cell with a 30 s vacuum cycle. A schematic of this procedure and the resulting cell stack structure is shown in Fig. 2.

2.2.3. Thermogravimetric analysis

Thermogravimetric analysis (TGA) was performed on a TA Instruments TGA 550 with a temperature range from room temperature (22 °C) to 250 °C at a ramp rate of 10 °C/min.

2.2.4. Ultraviolet-modulated rheology

A TA Instruments Discovery HR-2 rheometer was used in combination with a UV/Visible light curing accessory (OmniCure Series 2000) to evaluate the rheological properties of the HT-29 and FEC:FEMC 1 m LiTFSI gel electrolyte materials upon photo-induced polymerization at room temperature. The light source was filtered to 320–480 nm with the irradiation intensity set to 180 mW cm^{-2}. An oscillatory strain of 10% and a frequency of 1 Hz were used, with irradiation set to begin 30 s after the beginning of the experiment. The modulus crossover, or gel point, was recorded in duplicate.

2.2.5. UV–Vis spectrometry

Ultraviolet–visible (UV–Vis) spectrometry was performed with 350 μL samples with a 1 cm path length in Thor Labs small-sample fused quartz cuvettes. Samples were placed in a Thor Labs CVH100-CV blackout cuvette holder. A StellarNet deuterium/halogen source provided a spectrum of wavelengths from 190 nm to 1100 nm, and data was recorded using an Avantes AvaSpec 2048L detector. Samples were blanked using a dark (blocked) beam and an empty 1 cm path length fused quartz cuvette.

2.2.6. Battery impedance and cycle testing

Cells were held in custom-made pouch cell holders that applied ~2 PSI to the cell. A Solartron 1276/1280 device pair was used to collect electrochemical impedance spectroscopy (EIS) data. All EIS data was collected with the cells in the discharged state for the purposes of comparing a cycled cell with a freshly-built cell in the discharged state. Cells were scanned through a frequency range of 1 MHz–1 Hz at an amplitude of 10 mV with respect to the cell's open circuit potential. Battery cycling was performed on a Maccor 4000 battery tester with a custom constant current-constant voltage (CC-CV) test routine. Cells were initially tap-charged to 1 V, then allowed to rest for 3 h. Cells then underwent two CC-only forming cycle at C/10 rate from 4.2 V to 3.2 V. Once forming was complete, the cells cycled at C/10 from 4.2 V to 3.4 V followed by a constant voltage charge/discharge at the limit until either a current of C/50 was reached or 2 h had elapsed. Data analysis was

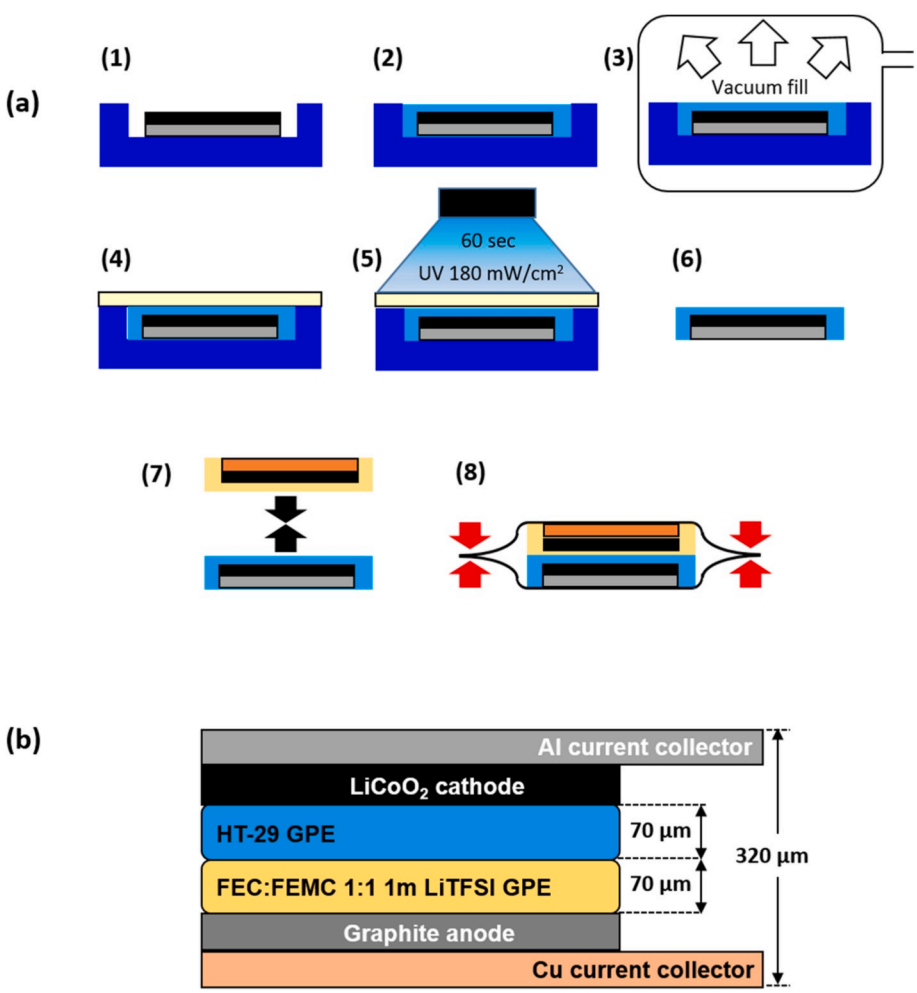

Fig. 2. (a) Schematic representation of the 4 V gel polymer electrolyte battery cell construction flow. (1) Cathode is placed in silicone mold, (2) electrolyte: polymer components are added, (3) 2 min vacuum fill to wet porous electrode, (4) placement of UV-transparent PTFE-coated glass slide, (5) 60 s. UV irradiation, (7) mating of gel-coated cathode and separately prepared gel-coated anode, (8) heat-sealing constructed stack in a pouch cell. (b) shows the schematic of the cell stack with approximately equal aqueous and non-aqueous GPE layer and total stack thickness.

performed using a custom analytical routine to process Maccor cycling and statistical output.

3. Results and discussion

It was found early in our work that acrylate electrolyte gels could be formed as long as the different components of the polymer were soluble in the electrolyte solution. This includes monomer, crosslinker, and initiator. MPEGA, HEA, the diacrylate crosslinker PEGDA700, and the initiator DMPA were all soluble in HT-29, and turned out also to be soluble in the FEC:FEMC 1 m LiTFSI electrolyte as well. The crosslinking of MPEGA/HEA/PEGDA700 gels was less effective in FEC:FEMC 1 m LiTFSI as compared to HT-29, with an 89:9:2 ratio of the three components resulting in a liquid product rather than a solid gel. PEGDA700 crosslinker was increased to 7 wt% with a corresponding decrease in MPEGA:HEA content, giving a solid gel product containing the FEC:FEMC 1 m LiTFSI electrolyte. The chemical structures of the polymer building blocks and a schematic of the MPEGA:HEA gel can be seen in Fig. 3.

Precision analysis by UV-cured rheology revealed several useful pieces of information related to the rates of polymerization of MPEGA:HEA:PEGDA700 in HT-29 and FEC:FEMC 1 m LiTFSI liquid electrolytes. Two competing factors were expected to be the effect of UV absorption by the solvent and the dependence of polymerization rate on the viscosity of the electrolyte. Fig. 4 shows the UV and near-UV absorbance of HT-29 and FEC:FEMC 1 m LiTFSI. DMPA in water has significant absorption peaks at 200 nm and 280 nm with an extended absorption region in the range of 310–370 nm implicated in DMPA radical formation [21]. The FEC:FEMC electrolyte, due to the presence of solvent carbonyl groups, absorbs fractionally more UV in the range 300–400 nm. The curing system utilizes primarily UV in the range 300 nm–400 nm where FEC:FEMC absorption is stronger than HT-29.

Fig. 5 and Table 1 detail the results of the UV-modulated rheology sample analysis. The point at which the storage modulus crosses the loss modulus, or modulus crossover, is indicative of the formation of a polymer network, or gel formation [22]. The HT-29 gel forms about 5 times more quickly than the FEC:FEMC 1 m LiTFSI gel, ~7 s compared with ~32 s after irradiation begins, respectively. This was initially a surprising result, as the liquid HT-29 resin prior to polymerization is more viscous than the FEC:FEMC 1 m LiTFSI electrolyte, with monomers/crosslinkers being equal in concentration in each unreacted solution. Given that HT-29 absorbance of curing UV radiation was lower than FEC:FEMC 1 m LiTFSI, it is very likely that the increased absorption of the FEC:FEMC electrolyte results in a reduced initiation rate, slowing polymerization and gelation kinetics with respect to the HT-29 solution. It is also possible that a carbonyl, such as FEC or FEMC, protonated during the initiator activation acts as a radical scavenger [23]. The simplest hypothesis is that UV absorption differences between the HT-29 and FEC:FEMC electrolytes lead to outsize kinetic effects during UV-initiated gel polymerization. Additionally, it was noted early in this

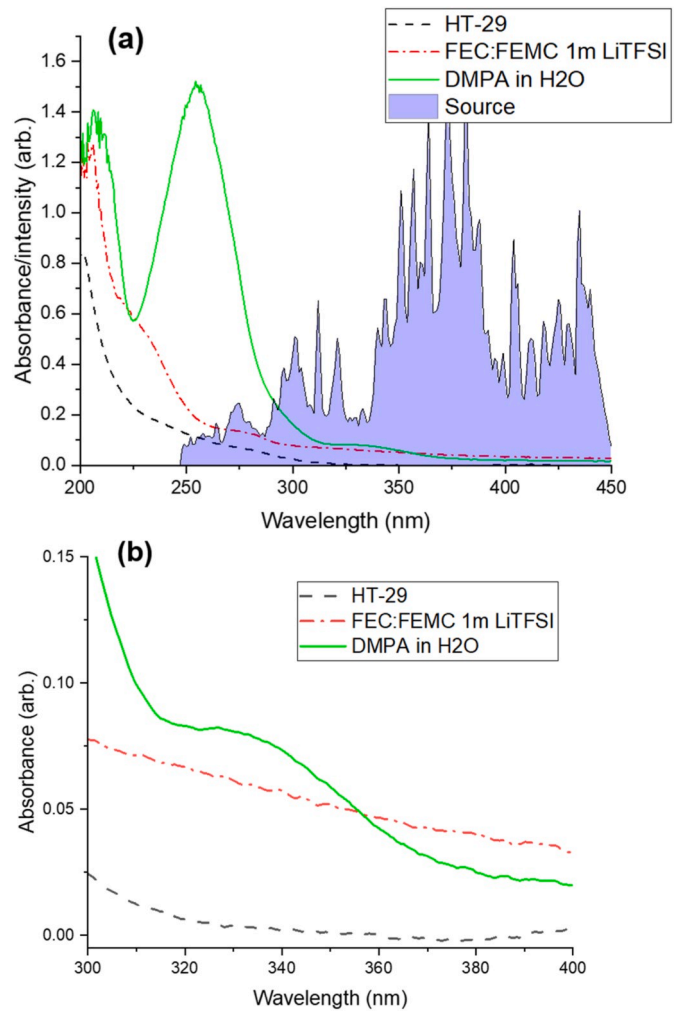

Fig. 4. (a) UV–Vis spectra of HT-29 electrolyte, FEC:FEMC 1 m LiTFSI, and DMPA 0.01% dissolved in water with UV source intensity overlaid. (b) Close-up of the 300–400 nm wavelength range to highlight the increased UV absorption of the FEC:FEMC 1 m LiTFSI electrolyte compared to HT-29.

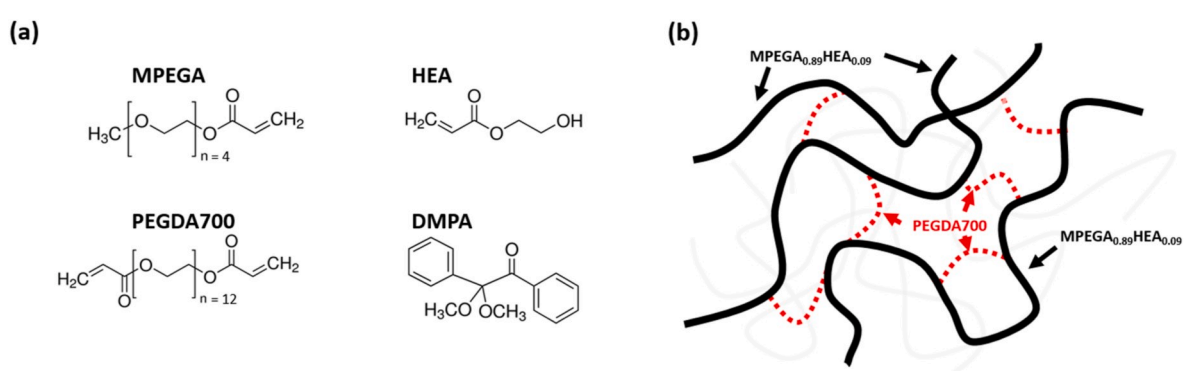

Fig. 3. (a) Structures of the two monomers MPEGA and HEA, the crosslinker PEGDA700, and the photoinitiator DMPA. (b) Schematic showing the copolymer MPEGA:HEA (black, solid) in the monomer ratio 89:9 for the HT-29 electrolyte gel with PEGDA700 (red, dotted) crosslinkers showing the possibility of both intra- and interchain connections that form the polymer network within the gel. (For interpretation of the references to color in this figure legend, the reader is referred to the Web version of this article.)

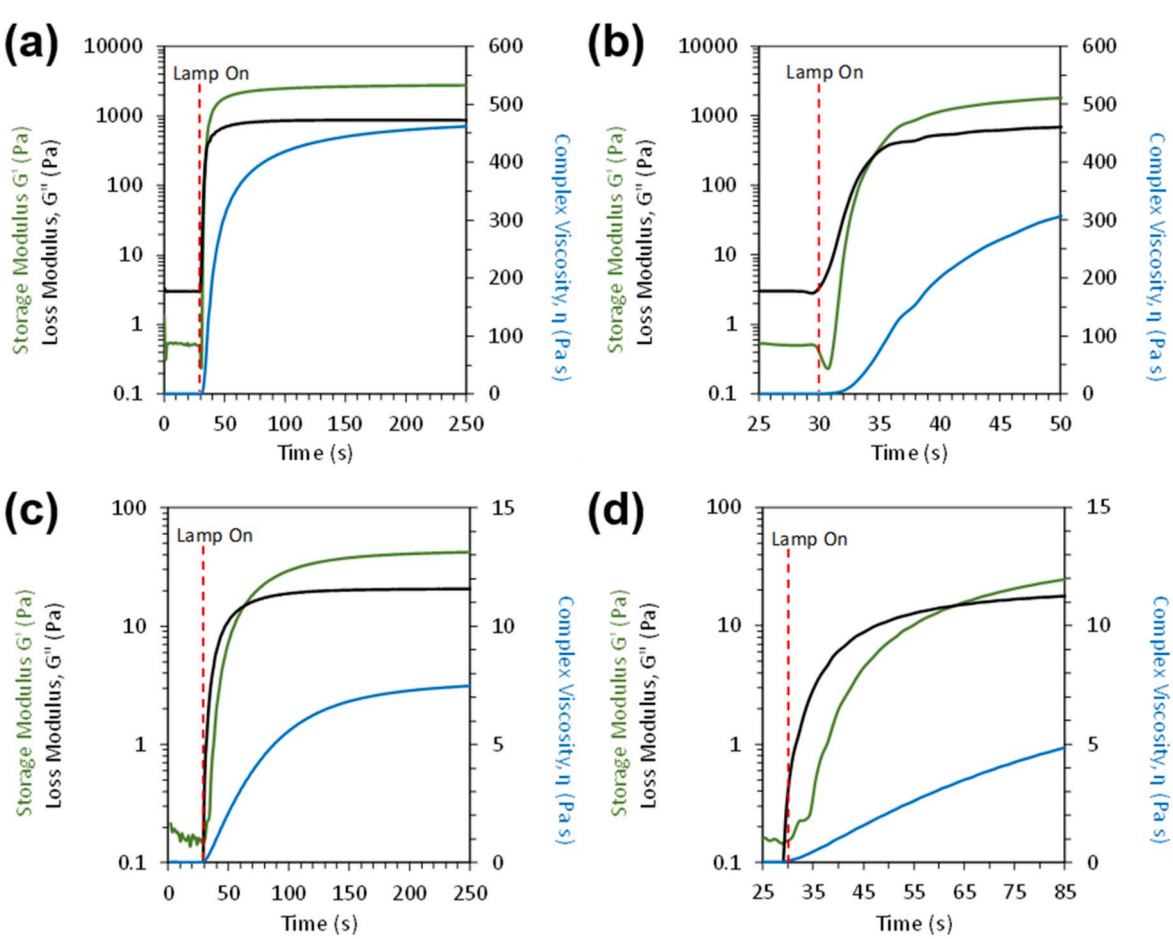

Fig. 5. UV-modulated rheology analysis of the a) HT-29, b) HT-29 zoomed for clarity, c) FEC:FEMC 1 m LITFSI gel electrolyte, and d) FEC:FEMC 1 m LITFSI gel electrolyte zoomed for clarity.

Table 1
Modulus crossover time (gel point, G′/G″) and plateau modulus (G′) at 3000 s for the HT-29 and FEC:FEMC 1 m LITFSI electrolytes.

Sample	Modulus Crossover (s)	Plateau Modulus (G′) @ 3000 s (x 10^5, MPa)
HT-29	7.28 ± 0.55	331.0 ± 17.0
FEC:FEMC 1 m LiTFSI	32.31 ± 3.14	7.4 ± 0.4

work that more crosslinker (PEGDA700) was necessary to solidify gels of FEC:FEMC 1 m. However, the increase in crosslinker content still led to overall lower modulus gels relative to HT-29, which could be a result of the FEC:FEMC electrolyte interfering with the photo-induced polymerization mechanism. If chain growth kinetics were retarded by the FEC:FEMC electrolyte, then increased crosslinker content would be necessary to have a greater chance of linking the slower-growing chains in solution. Furthermore, the HT-29 gel exhibits a substantially higher plateau modulus (G′) than the FEC:FEMC 1 m LiTFSI gel (Table [1]), which is likely a result of an increased degree of cure of the HT-29 polymer matrix, due to the aforementioned kinetic factors. The "softness", or low storage modulus, for both electrolyte gels is a critical factor in maintaining safety during violent damage: the gels deform readily but do not break or shatter, allowing them to maintain electrode coverage to prevent electrode contact and shorts.

In the gel network, both electrolytes exhibited limited mass loss in thermogravimetric analysis up to 100 °C with mass loss for the FEC:FEMC 1 m LiTFSI electrolyte increasing markedly above 100 °C due to FEMC evaporation. TGA results are plotted in Supplementary Fig. S1. Analysis of the TGA results suggest that the FEC:FEMC 1 m LiTFSI gel would be changing in composition above 100 °C operating temperature with loss of FEMC and may result in pressurization inside the pouch. However, limiting operation to even 90 °C with the current iteration of aqueous battery puts it in position to outperform state-of-the-art organic electrolyte batteries using $LiPF_6$ salt, which incur significant capacity and lifetime degradation penalties when operated close to a 70 °C temperature cap.

Conductivity data in Fig. 6 indicate that the HT-29 gel electrolyte has a conductivity of 0.3 mS/cm at room temperature in the MPEGA:HEA:PEGDA700 gel, lower than the typically measured value of 2.4 mS/cm at room temperature for liquid HT-29. In comparison, FEC:FEMC 1 m LiTFSI gel electrolyte had conductivity of 3 mS/cm at room temperature and higher Li^+ conductivity than the HT-29 gel electrolyte across the tested temperature range. It was found that the gel electrolytes deviated from strictly Arrhenius behavior at higher temperatures, and the dip in conductivity should be related to slow loss of solvent and increase in the gel polymer mass fraction. The FEC:FEMC electrolyte gel, with greater mass loss above 100 °C, deviated more sharply from the Arrhenius relation and resulted in artificially low activation energy calculation of 0.22 kJ/mol. The HT-29 gel electrolyte, by comparison, fitted more closely with an activation energy of 0.43 kJ/mol. Without FEC:FEMC mass loss, attributable to the volatile FEMC, limiting the fit to low temperature conductivity data results in an activation of energy of 12.42 kJ/mol. In the gel electrolyte, there is a more complicated relationship between Li^+ and its mobile and stationary Li^+ coordinating species. Considering that PEG groups attached to crosslinked acrylate

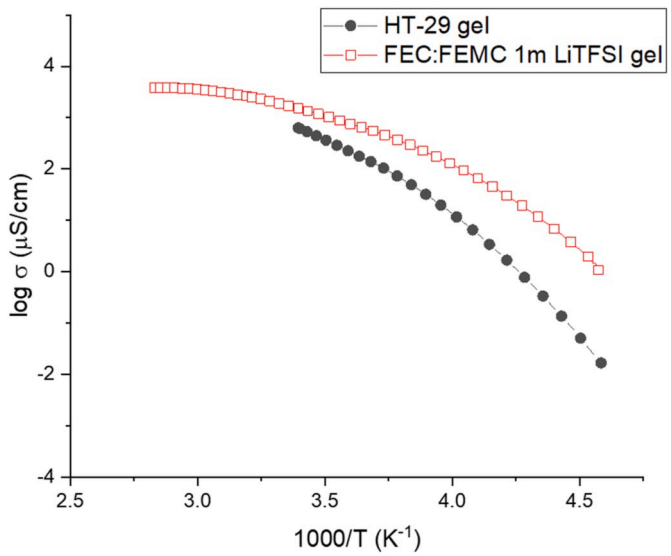

Fig. 6. Conductivity measurements for HT-29 and FEC:FEMC 1 m LITFSI electrolyte gels presented as an Arrhenius relation. Non-Arrhenius behavior at higher temperatures is attributed to solvent mass loss in the conductivity tester.

chains cannot reptate due to chain crosslinking, Li^+ association with these PEG groups should act to reduce overall Li^+ conductivity as observed. Previous work from our group showed that liquid-only HANE had supported high-rate cycling of 2C and above for a $Li_4Ti_5O_{12}$:$LiMn_2O_4$ electrode pair [15]. Transference number t_+ of WiSE and its derivative electrolytes are high, typically around 0.7[16] due to the fact that $Li^+(H_2O)_4$ complexes move and exchange in an effectively separate nanophase of the liquid electrolyte that is primarily composed of Li^+ and H_2O. The relationship between t_+ and conductivity should deviate from Nernst-Einstein behavior due to ion pairing and the separation of the Li_x-$(H2O)_y$ phase and the Li-poor Li_x-$TFSI_y$-$H2O_z$ phase [24], meaning that t_+ should influence Li^+ mobility as well as conductivity. As observed, the combination of modest conductivity and high t_+ allow useful cycling in HT-29 gels at room temperature.

Electrochemical impedance spectroscopy tests performed on as-built and cycled graphite-LCO pouch cells showed that the cells start off with a low internal resistance of 2.5 Ω, with typical data presented in Fig. 7. During cell cycling, the shape of the impedance curves changed such that the capacitors used to model as-built behavior had to be switched to constant phase elements (CPEs) to accurately capture cycled impedance behavior and derive meaningful resistance values. After 40 cycles, charge transfer resistance increases as indicated by the R2 value in Table 2, while overall cell resistance R1 decreases and interfacial resistance R3 increases by a factor of 1.72 but remains below 1 Ω. The low-frequency diffusion tail was not captured for the cycled cell, but the increased resistance caused by cycling should undoubtedly result in higher impedance associated with Li^+ diffusion. Low impedance growth for interfaces is considerably important to the cycling 4 V aqueous lithium-ion battery cell, as the need to protect the anode with the FEC:FEMC 1 m LiTFSI gel electrolyte introduces a third interface (the HT-29 gel electrolyte:FEC:FEMC gel electrolyte interface) into the system. EIS results before and after cycling make it clear that the liquid electrolyte components in the gel matrix allow sufficient Li^+ mobility and exchange between the two electrolytes and the electrodes.

The low resistance value and general impedance characteristics of the battery indicated that charging or discharging of the cell would not lead to unacceptable internal heating or charge transfer resistance, much like lithium-ion battery cells prepared with liquid carbonate electrolytes. Most importantly, these results indicate that there is relatively low charge-transfer resistance between the two gel electrolytes at their interface as well as the interfaces between each electrode and its

Table 2
Resistance values generated from model fitting for as-built and cycled pouch cells.

Sample	R1 (Ω)	R2 (Ω)	R3 (Ω)
As-built cell	2.363 ± 0.061	0.172 ± 0.004	0.331 ± 0.008
Cycled cell	0.989 ± 0.013	6.540 ± 1.937	0.570 ± 0.005

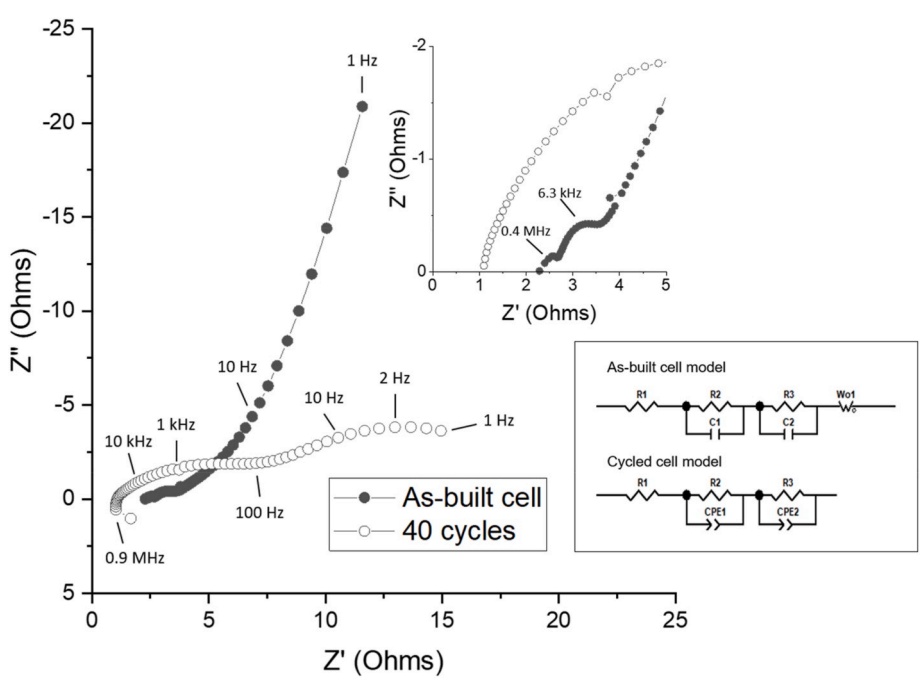

Fig. 7. EIS analysis of the HT-29/FEC:FEMC gel electrolyte battery as-built compared to the same cell after 40 cycles. Inset shows a close-up of the low Z′ region of the as-built cell to highlight its double-semicircle feature. Models used to develop values for cell (R1), charge transfer (R2), and interfacial (R3) are included in the boxed inset.

corresponding gel electrolyte. The same polymer components MPEGA:HEA:PEGDA700 in similar proportions are used in both the hydrophilic HT-29 electrolyte gel and the hydrophobic FEC:FEMC electrolyte gel, avoiding the potential for polymer de-wetting at the electrolyte-electrolyte interface. Full contact ensures effective Li^+ exchange across the interface, though this is a complex subject that merits more detailed investigation.

Pouch cells constructed using a matched graphite:LCO electrode pair presented several challenges to the gel electrolytes. Chief among these was the porous structure of the electrode, which had previously been used with liquid-like solids [18], and wetting of electrode pores was possible in that case. Regardless, partial wetting of the electrode surface area by the gel electrolytes was achieved, allowing charge/discharge cycling which is detailed in Fig. 8a–b. More than 50% of the cell capacity was available initially during cell testing.

The two main functions of the FEC:FEMC 1 m LiTFSI electrolyte were to passivate the graphite anode surface and prevent the reduction of water at the anode surface. An effective SEI caused by FEC:FEMC 1 m LiTFSI reduction is a combination of hydrophobic and hydrophilic components [25], though its primary component LiF is insoluble in water and has a high lattice energy, making it unfavorable for water to propagate with Li^+ in an LiF-rich SEI. Initially, Coulombic efficiency of the cycling cells reaches 99% before experiencing a decline after the 15th cycle. Such a high cycling efficiency could not be achieved if water was reduced at the anode, as its high mole fraction in the aqueous gel electrolyte (0.40) and the strength of the Li-water coordination would otherwise ensure enough water reached the anode to completely disable the cell on the first charge cycle, an issue encountered repeatedly during development. Rather, the primary contributor to performance decline was the limited areal contact between gel electrolyte and electrode material.

In order to diagnose electrode underutilization, a rest period was employed after charge and discharge steps to compare polarization of the electrodes, with the results plotted in Fig. 8d. The change in voltage after the discharge-rest cycle was higher than the change in voltage after charge-rest. Lithium-ion battery cells typically exhibit higher cell polarization in the charge step, resulting in a steeper decline in potential when charging current is removed. In that case, a greater potential drop would be expected on the charge cycle due to electrolyte decomposition and increased charge transfer resistance. Instead, what is observed in Fig. 8d is opposite: ΔV after CC-CV discharge starts at 250 mV and gradually reduces to 180 mV, where ΔV after CC-CV charge remains lower at a fairly steady 20 mV. The fact that the charge/discharge polarizations are different suggests that the process causing them has hysteresis-like behavior. It is most likely that the hysteresis involves the plating or loss of Li during the charge step followed by the inability to fully remove Li^+ from the anode due to losses from the previous charge step.

Therefore, the rest voltage change observation is a further indication that otherwise-stable interfaces are being subject to excessive current

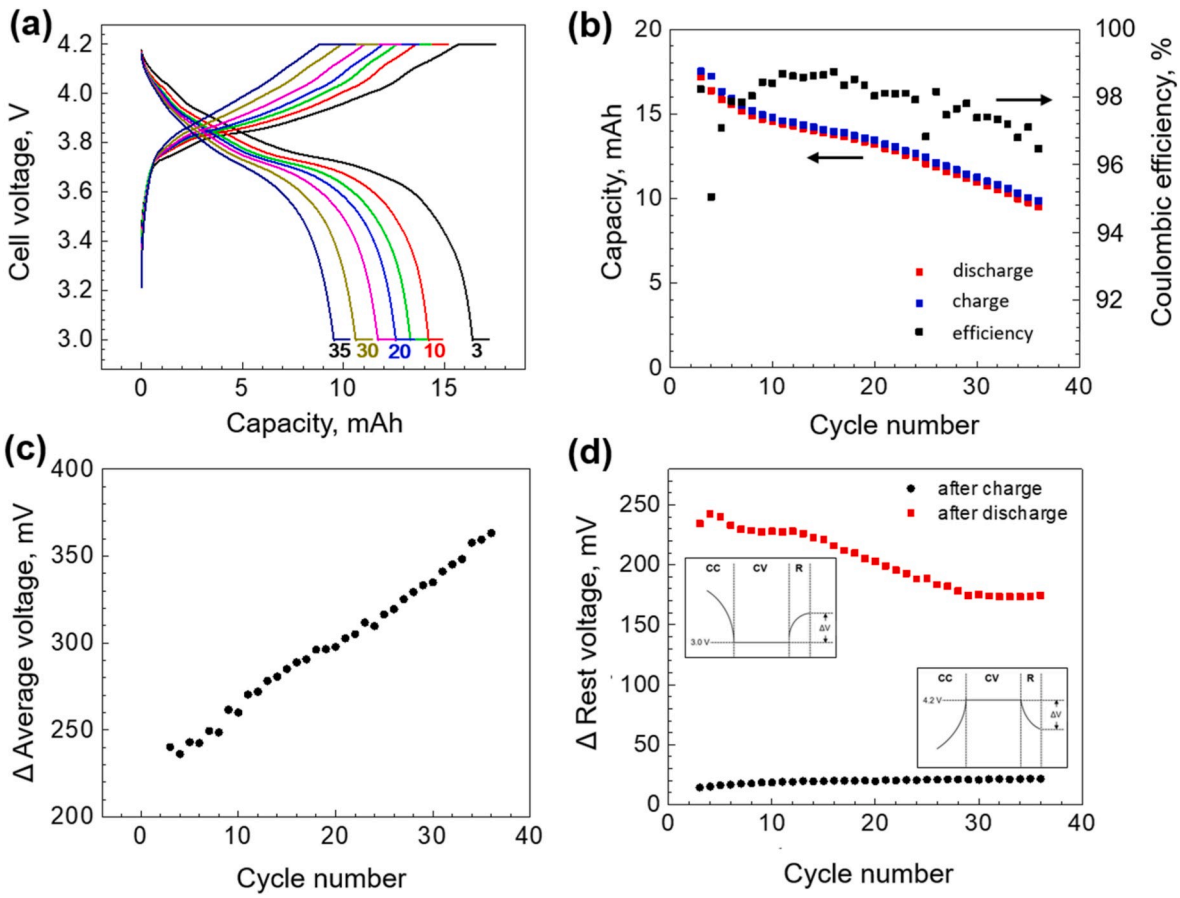

Fig. 8. Battery cycling results from HT-29-based gel electrolyte cell in a graphite-LCO cell, where (a) overlays several successive cycles as a function of capacity with the cycle number labeled below the corresponding curve, and (b) shows capacity and Coloumbic efficiency as a function of cycle number. (c) plots the difference between average charge and discharge voltage as a function of cycle number, with the rising value indicating polarization of the cell during cycling progression. (d) tracks polarization at the end of charge/discharge by comparing the potential at the end of the charge and discharge cycle with the potential following a 10 min rest after the charge and discharge cycle. Insets in Fig. 8d detail the progression from constant current (CC) step to constant voltage step (CV) to rest (R), and ΔV as the difference of target potential (3.0 V or 4.2 V) and potential at the end of the rest step. Smaller ΔV values indicate lower electrode polarization and more equilibrium-like electrode utilization.

due to limited contact between electrode materials and the gel electrolytes.

The point of using the HT-29 electrolyte, with non-flammable water and TMP solvents, was to remove the possibility of a battery fire resulting from damage to the cell, especially while the cell is at maximum charge. During cycling and while fully charged, battery cells constructed from graphite:LCO using HT-29 and FEC:FEMC 1 m LiTFSI gel electrolytes were able to continue cycling when cut in half, resisting the transient short of the scissor cut. The combination of non-flammable electrolytes with a compliant but sufficiently strong gel polymer network results in a separator-free electrolyte system that is tolerant of blunt, cutting, and penetrating damage, and one that cannot act as fuel for an overheated battery. The MPEGA:HEA gel electrolyte allows high strains in excess of 5% and has a low storage modulus of 3–3.5 kPa. The combination of low storage modulus and high strain tolerance allows the gels to deform and accept physical damage without uncovering and exposing bare electrode material, causing internal shorting. The high temperature stability of the LiTFSI salt and limitations placed on liquid component volatility ensure that high temperature environments pose less threat to the battery described in this paper compared to modern state-of-the-art lithium-ion batteries. Going forward, the arrangement of aqueous electrolyte interfacing with a lithium or lithium-potential-like anode through a thin hydrophobic electrolyte is expected to produce cells with reducing packaging requirements that should be able to cross the 300 Wh/kg threshold in pursuit of a flexible, non-flammable 400 Wh/kg cell.

4. Conclusions

Presented in this work is a new type of lithium ion battery that combines aqueous and non-aqueous electrolyte gels in an easily manufactured and non-flammable system that allows a 4V operating potential and resists violent failure upon damage. These gels retain the useful properties of the liquid electrolyte phase while physically containing the liquid electrolyte in a flexible, damage-resistant polymer network. Acrylate gels are easily processed using existing ultraviolet curing techniques, and could be adapted to high-throughput manufacturing. In this work, gel electrolytes based on PEG-containing acrylates were made from the hybrid aqueous HT-29 and the carbonate electrolyte FEC:FEMC 1 m LiTFSI. Polymerizations in HT-29 were rapid with gelation taking roughly 6 s, while polymerizations in FEC:FEMC 1 m LiTFSI was slower, taking about 35 s to complete. The finished gels had low storage/loss moduli that allowed them to deform with damage and allowed a fully cut-open cell to continue cycling. Cells were cycled against porous graphite:LCO electrodes and allowed charging and discharging of the electrodes, promising a robust and damage-resistant 4V-class lithium ion battery that is easily manufactured and with a wide application domain.

Declaration of competing interest

The authors declare that they have no known competing financial interests or personal relationships that could have appeared to influence the work reported in this paper.

CRediT authorship contribution statement

Arthur Cresce: Writing - original draft, Writing - review & editing, Project administration, Conceptualization, Methodology, Investigation, Formal analysis, Data curation, Visualization, Funding acquisition. **Nico Eidson:** Writing - review & editing, Conceptualization, Methodology, Data curation. **Marshall Schroeder:** Methodology, Investigation, Validation. **Lin Ma:** Conceptualization, Investigation, Validation. **Yakira Howarth:** Project administration, Funding acquisition, Conceptualization, Supervision. **Chongyin Yang:** Conceptualization, Methodology, Investigation, Formal analysis. **Janet Ho:** Conceptualization, Methodology, Investigation. **Robert Dillon:** Writing - review & editing, Conceptualization, Formal analysis. **Michael Ding:** Investigation, Formal analysis, Visualization. **Alexander Bassett:** Methodology, Investigation, Formal analysis, Visualization. **Joseph Stanzione:** Writing - original draft, Writing - review & editing, Conceptualization, Investigation. **Robinson Tom:** Conceptualization, Investigation. **Thiagarajan Soundappan:** Conceptualization, Investigation, Formal analysis. **Chunsheng Wang:** Conceptualization, Methodology, Supervision. **Kang Xu:** Writing - original draft, Writing - review & editing, Conceptualization, Methodology, Formal analysis, Visualization, Supervision.

Acknowledgements

The authors would like to acknowledge the FY19 funding grant from the US Army Research Lab which supported this work. The authors would also like to acknowledge the collaborative effort of the Johns Hopkins University Applied Physics Laboratory. Dr. Lin Ma acknowledges the Army Research Laboratory for providing financial support under the Dr. Brad. E. Forch Distinguished Postdoctoral Fellowship administered by the National Research Council.

Appendix A. Supplementary data

Supplementary data to this article can be found online at https://doi.org/10.1016/j.jpowsour.2020.228378.

References

[1] M.W. Shinwari, D. Zhitomirsky, I.A. Deen, P.R. Selvaganapathy, M.J. Deen, D. Landheer, Microfabricated reference electrodes and their biosensing applications, Sensors (Basel) 10 (3) (2010) 1679–1715.
[2] D.W. Kimmel, G. LeBlanc, M.E. Meschievitz, D.E. Cliffel, Electrochemical sensors and biosensors, Anal. Chem. 84 (2) (2012) 685–707.
[3] R. Thrier, S. Buschor, H. Buhrer, H. Buhler, Polym. Electrolyte 6 (2002), 468,408.
[4] P.R. Warburton, M. Zamanzadeh, Reference Electrode, 2005.
[5] A.K. Arof, I.M. Noor, M.H. Buraidah, T.M.W.J. Bandara, M.A. Careem, I. Albinsson, B.E. Mellander, Polyacrylonitrile gel polymer electrolyte based dye sensitized solar cells for a prototype solar panel, Electrochim. Acta 251 (2017) 223–234.
[6] S.E. Gledhill, B. Scott, B.A. Gregg, Organic and nano-structured composite photovoltaics: an overview, J. Mater. Res. 20 (12) (2005) 3167–3179.
[7] W. Glasspool, J. Atkinson, A screen-printed amperometric dissolved oxygen sensor utilising an immobilized electrolyte gel and membrane, Sensor. Actuator. B 48 (1998) 308–317.
[8] M. Armand, Polymer solid electrolytes - an overview, Solid State Ionics 9–10 (1983) 745–754.
[9] M.B. Armand, M.J. Duclot, P. Rigaud, Polymer solid electrolytes - stability domain, Solid State Ionics 3–4 (AUG) (1981) 429–430.
[10] J.B. Goodenough, Y. Kim, Challenges for rechargeable Li batteries, Chem. Mater. 22 (3) (2010) 587–603.
[11] P.G. Bruce, B. Scrosati, J.M. Tarascon, Nanomaterials for rechargeable lithium batteries, Angew. Chem. Int. Ed. 47 (16) (2008) 2930–2946.
[12] D.C. Lin, Y.Y. Liu, Y. Cui, Reviving the lithium metal anode for high-energy batteries, Nat. Nanotechnol. 12 (3) (2017) 194–206.
[13] C. Yang, J. Chen, X. Ji, T.P. Pollard, X. Lü, C.-J. Sun, S. Hou, Q. Liu, C. Liu, T. Qing, Y. Wang, O. Borodin, Y. Ren, K. Xu, C. Wang, Aqueous Li-ion battery enabled by halogen conversion–intercalation chemistry in graphite, Nature 569 (7755) (2019) 245–250.
[14] L. Suo, O. Borodin, T. Gao, M. Olguin, J. Ho, X. Fan, C. Luo, C. Wang, K. Xu, "Water-in-salt" electrolyte enables high-voltage aqueous lithium-ion chemistries, Science 350 (6263) (2015) 938–943.
[15] F. Wang, O. Borodin, M.S. Ding, M. Gobet, J. Vatamanu, X. Fan, T. Gao, N. Eidson, Y. Liang, W. Sun, S. Greenbaum, K. Xu, C. Wang, Hybrid aqueous/non-aqueous electrolyte for safe and high-energy Li-ion batteries, Joule 2 (5) (2018) 927–937.
[16] O. Borodin, L. Suo, M. Gobet, X. Ren, F. Wang, A. Faraone, J. Peng, M. Olguin, M. Schroeder, M.S. Ding, E. Gobrogge, A. von Wald Cresce, S. Munoz, J.A. Dura, S. Greenbaum, C. Wang, K. Xu, Liquid structure with nano-heterogeneity promotes cationic transport in concentrated electrolytes, ACS Nano 11 (10) (2017) 10462–10471.
[17] O. Borodin, L. Suo, M. Olguin, A.v. Cresce, J. Vatamanu, F. Wang, X. Ren, J. A. Dura, A. Faraone, M. Gobet, In Structure and Transport of "Water-In-Salt" Electrolytes from Molecular Dynamics Simulations, Electrochemical Society Meeting Abstracts, The Electrochemical Society, 2017, 2014-2014.
[18] C. Yang, J. Chen, T. Qing, X. Fan, W. Sun, A. von Cresce, M.S. Ding, O. Borodin, J. Vatamanu, M.A. Schroeder, N. Eidson, C. Wang, K. Xu, 4.0 V aqueous Li-ion batteries, Joule 1 (1) (2017) 122–132.

[19] UV-curable inkjet inks and their applications in industrial inkjet printing, including low-migration inks for food packaging. In Handbook of Industrial Inkjet Printing, pp 129-150.
[20] J.W. Vanderhoff, Ultraviolet light cured inks—a review, in: Ultraviolet Light Induced Reactions in Polymers, vol. 25, AMERICAN CHEMICAL SOCIETY, 1976, pp. 162–187.
[21] V. Mucci, C. Vallo, Efficiency of 2,2-dimethoxy-2-phenylacetophenone for the photopolymerization of methacrylate monomers in thick sections, J. Appl. Polym. Sci. 123 (1) (2012) 418–425.
[22] C.-Y.M. Tung, P.J. Dynes, Relationship between viscoelastic properties and gelation in thermosetting systems, J. Appl. Polym. Sci. 27 (2) (1982) 569–574.
[23] L. Pitzer, F. Sandfort, F. Strieth-Kalthoff, F. Glorius, Intermolecular radical addition to carbonyls enabled by visible light photoredox initiated hole catalysis, J. Am. Chem. Soc. 139 (39) (2017) 13652–13655.
[24] N. Boden, S.A. Leng, I.M. Ward, Ionic conductivity and diffusivity in polyethylene oxode/electrolyte solutions as models for polymer electrolytes, Solid State Ionics 45 (3) (1991) 261–270.
[25] X. Fan, L. Chen, O. Borodin, X. Ji, J. Chen, S. Hou, T. Deng, J. Zheng, C. Yang, S. C. Liou, K. Amine, K. Xu, C. Wang, Non-flammable electrolyte enables Li-metal batteries with aggressive cathode chemistries, Nat. Nanotechnol. 13 (8) (2018) 715–722.